



Contents lists available at ScienceDirect

Journal of Rock Mechanics and Geotechnical Engineering

journal homepage: www.jrmge.cn

Full Length Article

Laboratory-scale investigation of response characteristics of liquid-filled rock joints with different joint inclinations under dynamic loading

Jin Huang^a, Xiaoli Liu^{a,*}, Danqing Song^a, Jian Zhao^b, Enzhi Wang^a, Jianmin Zhang^a^a State Key Laboratory of Hydrosience and Engineering, Tsinghua University, Beijing, 100084, China^b Department of Civil Engineering, Monash University, Clayton, VIC, 3800, Australia

ARTICLE INFO

Article history:

Received 5 May 2021

Received in revised form

8 July 2021

Accepted 20 August 2021

Available online 23 November 2021

Keywords:

Liquid-filled rock joint

Stress wave

Laboratory investigation

Wave propagation characteristics

Liquid dynamic response

ABSTRACT

In underground rock engineering, water-bearing faults may be subjected to dynamic loading, resulting in the coupling of hydraulic and dynamic hazards. Understanding the interaction mechanism between the stress waves induced by dynamic loadings and liquid-filled rock joints is therefore crucial. In this study, an auxiliary device for simulating the liquid-filled layer was developed to analyze the dynamic response characteristics of liquid-filled rock joints in laboratory. Granite and polymethyl methacrylate (PMMA) specimens were chosen for testing, and high-amplitude shock waves induced by a split Hopkinson pressure bar (SHPB) were used to produce dynamic loadings. Impact loading tests were conducted on liquid-filled rock joints with different joint inclinations. The energy propagation coefficient and peak liquid pressure were proposed to investigate the energy propagation and attenuation of waves propagating across the joints, as well as the dynamic response characteristics of the liquid in the liquid-filled rock joints. For the inclination angle range considered herein, the experimental results showed that the energy propagation coefficient gently diminished with increasing joint inclination, and smaller coefficient values were obtained for granite specimens compared with PMMA specimens. The peak liquid pressure exhibited a gradually decreasing trend with increasing joint inclination, and the peak pressure for granite specimens was slightly higher than that for PMMA specimens. Overall, this paper may provide a considerably better method for studying liquid-filled rock joints at the laboratory scale, and serves as a guide for interpreting the underlying mechanisms for interactions between stress waves and liquid-filled rock joints.

© 2022 Institute of Rock and Soil Mechanics, Chinese Academy of Sciences. Production and hosting by Elsevier B.V. This is an open access article under the CC BY-NC-ND license (<http://creativecommons.org/licenses/by-nc-nd/4.0/>).

1. Introduction

Underground rock engineering projects in China are increasingly being conducted in the western mountainous and karst areas, which comprise complicated terrain and geological conditions and exhibit the following main characteristics: large embedded depth, long cave line, high ground stress, high water pressure, strong karst, complex structure, and frequent disasters (Cook, 1992; Barton, 2002; Berkowitz, 2002; Hajiabdolmajid and Kaiser, 2003; Zhu et al., 2010; Li et al., 2013; Ma et al., 2015; Qian and Zhou, 2018; Chen et al., 2020). Underground rock engineering projects, such as traffic or diversion tunnels, underground storage caverns, and

underground mining, are often affected by geological disasters, such as collapse and instability of surrounding rocks (Martino and Chandler, 2004; Yang et al., 2017; Wang et al., 2018), inrush of mud or water (Li et al., 2016a, 2020; Zhang et al., 2018), rock bursts (Ortlepp and Stacey, 1994; Xiao et al., 2016; Manouchehrian and Cai, 2017; Ma et al., 2018; Zhao et al., 2020), and gas outbursts (Flores, 1998; Li and Hua, 2006; Zhou et al., 2020a) during construction and operation. It is of great practical significance to study the mechanisms of disasters that affect underground rock engineering projects (Watanabe et al., 1992; Li et al., 2016b; Liu et al., 2018; Liu et al., 2020a). In terms of multimode disasters, hydraulic–dynamic hazards are prominent, and the study of dynamic responses of water-bearing faults is of great value in the field of underground engineering, as illustrated in Fig. 1.

Considering rock engineering under complicated geological conditions, water-bearing faults and dynamic loadings often occur simultaneously. Dynamic loading is a common factor for initiation of disasters affecting underground rock engineering projects,

* Corresponding author.

E-mail address: xiaoli.liu@tsinghua.edu.cn (X. Liu).

Peer review under responsibility of Institute of Rock and Soil Mechanics, Chinese Academy of Sciences.

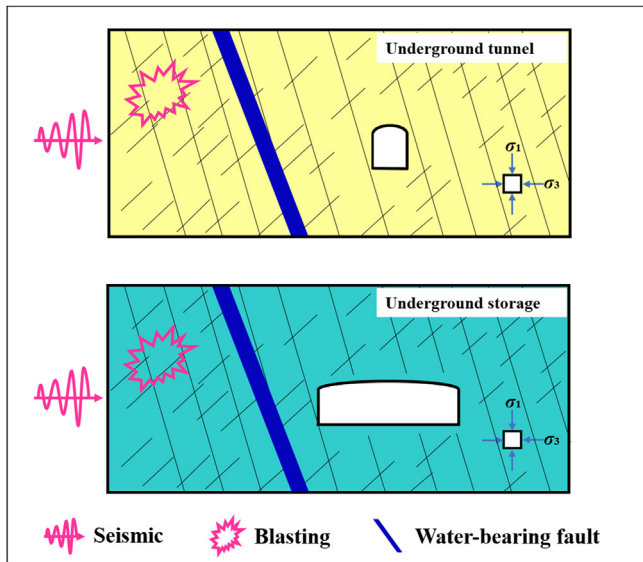


Fig. 1. Schematic diagram of rock dynamic problems for classic underground engineering involving water-bearing faults.

particularly in the form of stress waves propagating through water-bearing faults, which lead to complex interactions between waves and fault structures. The original hydraulic–mechanical balance system is disrupted by the inconsistent responses of the liquid and rock mass to the stress wave, resulting in abrupt changes in stress and seepage fields in the affected area (Liu et al., 2015; Sun et al., 2019). Disruption of the hydraulic–mechanical balance triggers the dynamic response of the surrounding rock system and intensifies crack proliferation in the rock mass. This induces the formation of leakage channels and results in the coupling of hydraulic–dynamic hazards to underground engineering projects (Wei et al., 2017; Liu et al., 2019; Han et al., 2020a).

In laboratory-scale investigations, rock specimens are typically used in dynamic loading analyses to examine rock dynamic problems in underground rock engineering (Zhao et al., 1999; Li et al., 2005; Dai et al., 2010; Wu et al., 2016; Fan et al., 2017; Zhu et al., 2020). Many studies have been carried out on stress wave propagation in jointed rock masses (Watanabe and Sassa, 1995; Li et al., 2011, 2018a, 2019a; Wu et al., 2013; Huang et al., 2016; Han et al., 2020b), and investigation of phenomena such as the dynamic properties of rock materials at high strain rates (Goldsmith et al., 1976; Frew et al., 2001; Zhao et al., 2014; Si et al., 2019; Ma et al., 2020), as well as the dynamic fracture behavior and failure criteria of rock (Xia et al., 2008; Dai et al., 2016; Zou et al., 2016; Wang et al., 2017; Zhou et al., 2020b). Pyrak-Nolte et al. (1990) investigated compressive and shear wave transmission through natural fractures in rock specimens under saturated and dry conditions. Li et al. (2019b) conducted dynamic tests to study the influence of joint roughness on wave attenuation in rock masses. Ju et al. (2007) proposed a fractal geometry approach to analyze the effects of rough surfaces on wave propagation. The mechanical behavior of a rock material is sensitive to the loading rate. Perkins et al. (1970) used dynamic experiments to demonstrate that tonalite specimens exhibit maximum stress with increasing strain rate. Zhao and Li (2000) used the Brazil method and 3-point flexural method to test granite and found that the dynamic tensile strength increased with increasing loading rate. Pei et al. (2020) analyzed the dynamic tensile response of sandstone specimens under static pre-tension at various loading rates. Fracture patterns and failure

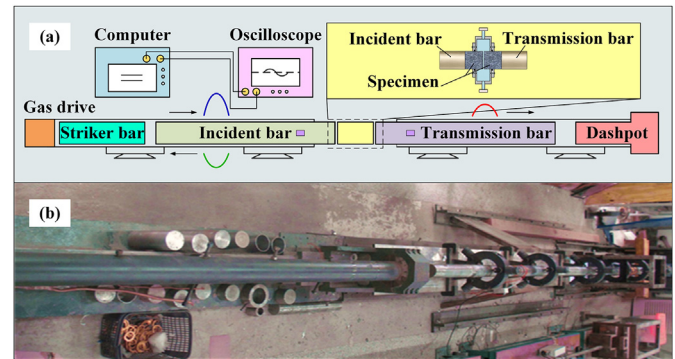


Fig. 2. Experimental setup for the study: (a) Principle diagram of the test system; and (b) Image of the dynamic loading device.

processes are important for studying the dynamic characteristics of rock materials. Klepaczko et al. (1984) provided information on the dynamic fracture properties of coal specimens, which served as a reference for finite element analyses of such materials. Li et al. (2018b) presented a unified scaling law to represent the dynamic behavior of rocks and provide information concerning grain-scale fractures.

In the dynamic response testing of water-bearing rock mass structures, it is worth analyzing the similar simulation model for liquid-filled rock joints that use liquid as the filling material. For the study of liquid-filled rock joints, recently published results have investigated diverse factors, such as the filling liquid type, filling liquid thickness, and liquid content, under different types of wave signals (Yang et al., 2019, 2020; Huang et al., 2020). Nevertheless, most studies have focused on wave propagation across single vertical or horizontal rock joints filled with liquid. However, joint inclinations have not been adequately investigated, wherein there is a greater degree of applicability and complexity. In addition, previous studies have mainly concentrated on low-amplitude ultrasonic waves propagating through liquid-filled rock joints; however, the dynamic response of the filling liquid during the dynamic loading process was not fully considered. Further research on the effects of shock waves with higher amplitudes on liquid-filled joints with various inclinations could more effectively strengthen the universal connection between laboratory research and engineering practice. Therefore, a better understanding of the hydraulic–dynamic coupling hazard mechanism in underground rock engineering may be realized.

Based on the current research progress, an auxiliary device was developed in this study to model liquid-filled rock joints and analyze the dynamic response characteristics of granite and polymethyl methacrylate (PMMA) specimens in laboratory-scale investigations. Two parameters for characterizing the main dynamic behaviors, i.e. the energy propagation coefficient and peak liquid pressure, were introduced in this study. The split Hopkinson pressure bar (SHPB) testing system was employed to simulate dynamic loading in underground rock engineering. A series of impact tests on liquid-filled rock joints with different joint inclinations was conducted in the laboratory. Using the experimental data collected in the dynamic tests, the wave energy propagation and response of the filling liquid were evaluated quantitatively, and the physical mechanisms underlying the above results involving shock waves, oblique jointed rock masses, and liquid in the joints of the rock masses were subsequently discussed. The study results may provide a better method for studying liquid-filled rock joints to gain a deeper understanding of the coupling of hydraulic–dynamic hazards in underground engineering.

2. Experiments and methodology

2.1. Experimental apparatus

The development of testing techniques for dynamic experiments has greatly aided the study of dynamic behaviors of rock-like materials and rock mass structures. In this study, the SPHB (Fig. 2) was chosen as the source of dynamic loading. It is usually composed of a striker bar, incident bar, transmission bar, and data acquisition system, which has been widely used for high strain rate testing (Hopkinson, 1872, 1914; Kolsky, 1949; Howe et al., 1974; Field et al., 2004; Li et al., 2009, 2013; Dai et al., 2010; Xia and Yao, 2015; Wen et al., 2020; Jiang et al., 2021).

A liquid-filling auxiliary device was developed to simulate liquid-filled rock joints in the laboratory tests, as illustrated in Fig. 3. The auxiliary device, consisting primarily of a metallic cavity, a pair of metal flanges associated with rubber sealing rings, two metal ball valves, and a dynamic sensor, was used in combination with the SPHB to produce dynamic loading of the liquid-filled rock joints. Holes were made on both sides of the cavity to mount the test specimens, and sealing rings were fixed in place with flanges to avoid leakage of the filling fluid. A dynamic sensor with an installation size of $M10 \times 1$ mm was placed in a hole along the sidewall of the metallic cavity to instantaneously collect the liquid pressure signal during the experimental process.

2.2. Specimen preparation

The granite specimens were cored and manufactured from an intact granite block obtained from Gansu Province, China. The two flat-end surfaces of the granite specimens were machined and polished to a roughness of less than 0.02 mm to ensure good contact between the specimens and bars of the SHPB. The average diameter and height of the cylindrical specimens were 63 mm and 126 mm, respectively. The specimens were cut at angles of 0° , 10° , 20° , and 30° in the center, and the cutting surfaces were used to simulate joint surfaces. The angles were obtained by controlling the angle between the cutting surface and circumferential surface normal lines. The apertures of artificial joints sandwiched between two cylindrical rock materials were adjusted to the same value (3 mm in this study) and were used for filling with fluid to obtain liquid-filled rock joints with different joint inclinations, as shown in Fig. 4. To further minimize the variation in granite properties across the specimen set and the dispersion of experimental data, PMMA was processed to the same size as the granite due to its good isotropy and homogeneity. Water was chosen as the filling fluid in this study. The physico-mechanical parameters of the different materials used in the test are listed in Table 1.

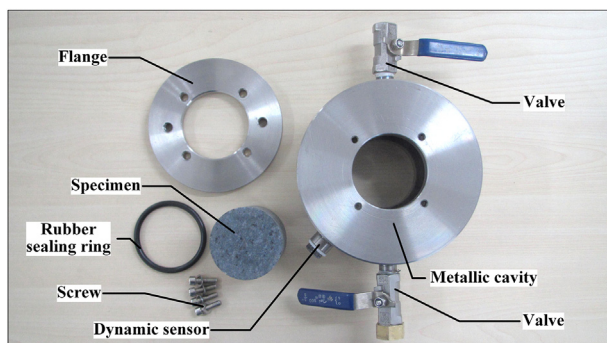


Fig. 3. Liquid-filling auxiliary device.

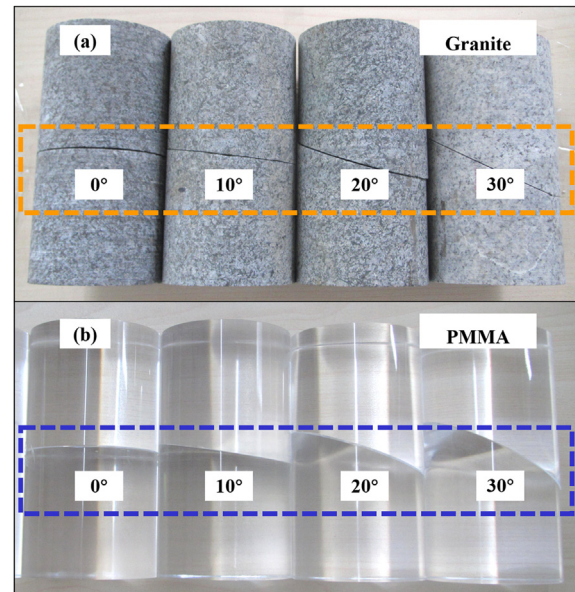


Fig. 4. Granite and PMMA specimens for dynamic loading.

2.3. Test procedures

Feasibility verification of the liquid-filling auxiliary device was first carried out under a series of testing conditions. Typical signal curves for the specimens were compared to demonstrate that the liquid-filling auxiliary device did not have a large impact on the test; therefore, the auxiliary device was considered feasible and acceptable (Huang et al., 2020). Each test was divided into three procedures: specimen installation, liquid injection, and dynamic loading. The main process of specimen installation is illustrated in Fig. 5, in which granite material was used as an example for the liquid-filling auxiliary device. Joint inclinations of 0° , 10° , 20° , and 30° with constant initial filling liquid thickness were tested to investigate the effects of joint inclination on the response characteristics of oblique liquid-filled rock joints under dynamic loading. Subsequently, a series of steps for injection of filling liquid was designed and conducted as follows: (i) the injection valve near the dynamic sensor was opened, and the outlet valve was closed; (ii) the metallic cavity of the liquid-filling auxiliary device was filled with water using a syringe; (iii) the outlet valve was immersed in a sink containing water firstly and then opened; (iv) the syringe was used to suck the liquid into the cavity and train away the liquid through the conduit; and (v) the suction operation was repeated three to five times to ensure that the cavity had been filled with liquid and to reduce interference from bubbles during testing. Ultimately, the liquid-filling auxiliary device with the specimens and filling liquid was sandwiched between the incident and transmission bars of the SHPB, as shown in Fig. 6. The strain signals from the bars and the liquid pressure of the total testing process were recorded using strain gauges and dynamic sensors. In addition, six tests were performed repeatedly for each case to minimize possible operational and measurement errors in the testing procedures.

3. Test results and discussion

3.1. Parameters for characterizing the main dynamic behaviors

3.1.1. Energy propagation coefficient

To investigate the mechanisms underlying the coupling of hydraulic-dynamic hazards induced by dynamic loading in

Table 1
Parameters of the different materials used in the experiment.

Material	Density (kg/m ³)	Young's modulus (GPa)	Bulk modulus (GPa)	Poisson's ratio	Uniaxial compressive strength (MPa)	Longitudinal wave velocity (m/s)
Granite	2600	63	—	0.28	154	4300
PMMA	1200	3	—	0.35	—	2700
Water	1000	—	2	—	—	1500

Note: Data for granite and PMMA specimens are listed with average values. Water was chosen as the filling fluid, and its relevant properties were taken at room temperature (20 °C).

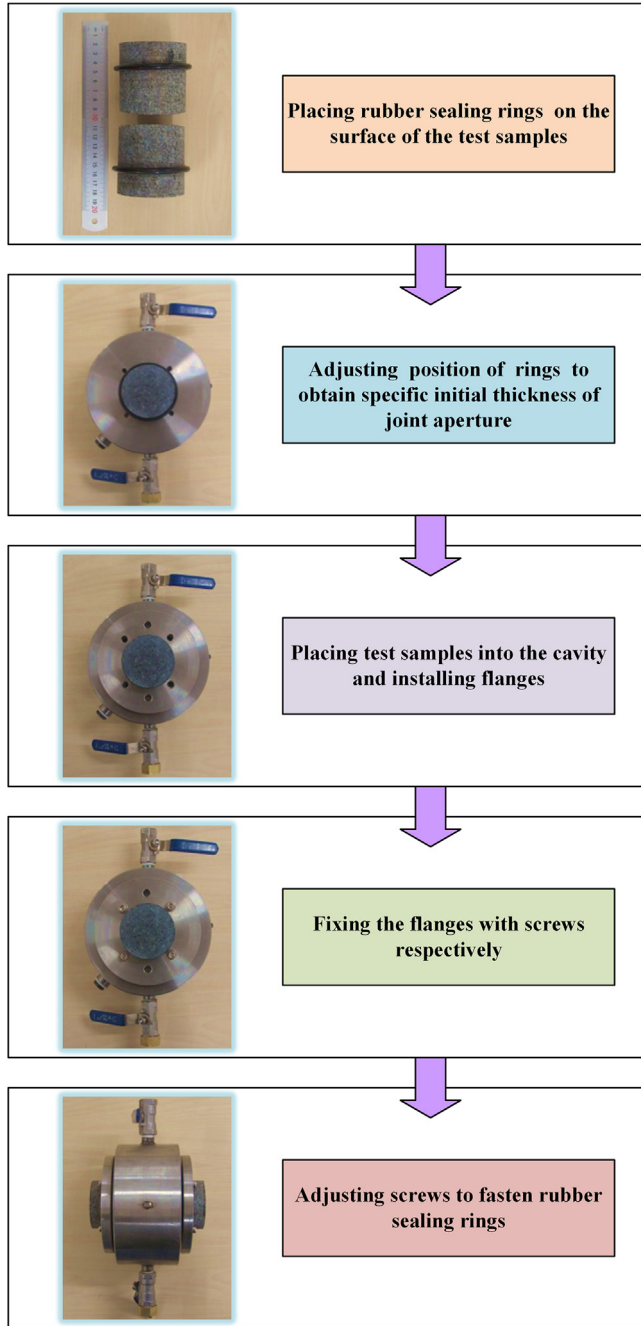


Fig. 5. Workflow of specimen installation for the liquid-filling auxiliary device (after Huang et al., 2020).

underground rock engineering, it is vital to examine the roles of energy propagation and attenuation. In this experimental study, the energy propagation coefficient is defined as the ratio of the

signal amplitudes of the first arriving wave of the transmission bar to that of the incident bar, which is used to describe the energy variation in wave propagation through liquid-filled rock joints. It is worth noting that the amplitude of the transmission wave is relatively small owing to the wave impedance mismatch in the sandwich structure, which is obtained by an amplification factor multiplied by the strain value of transmission signal. A difference of the wave impedance in the contact surfaces between the metal bars and specimens existed, which might have an impact on analyses of the results, as shown in Fig. 7. A series of correction tests with different specimen materials was carried out to analyze the effects of the difference, and further details of this investigation procedure can be found in Huang et al. (2020). The formulas for calculating the energy propagation coefficient are as follows:

$$E_{n,original} = E_{n,uncorrected} = \frac{\varepsilon_t}{\varepsilon_i} = \frac{k\varepsilon_{t,original}}{\varepsilon_{i,original}} \quad (1)$$

$$\Delta E_{n,metal-material} + \Delta E_{n,liquid} + E_{n,uncorrected} = 1 \quad (2)$$

$$\Delta E_{n,liquid} + E_{n,corrected} = 1 \quad (3)$$

$$E_{n,corrected} = E_{n,uncorrected} + \Delta E_{n,metal-material} \quad (4)$$

where $E_{n,original}$ is the original value of the energy propagation coefficient without correcting for the effects of the contact surfaces; ε_t and ε_i are the signal amplitudes of the transmission and incident bars, respectively, wherein the subscript 'original' denotes the values obtained directly from the original experimental data; k is the amplification factor, which is 5 in this study for the appropriate enlargement of the transmission signals to facilitate analysis; $\Delta E_{n,metal-material}$ and $\Delta E_{n,liquid}$ are the increments of the energy propagation coefficient caused by the surface between the metal bars and specimen and by the filling liquid layer, respectively; and $E_{n,corrected}$ represents the value of energy propagation coefficients following correction tests considering the effects of contact

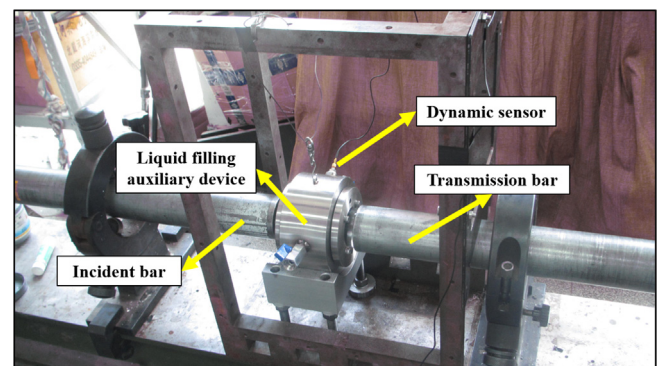


Fig. 6. Photographic views of installation for the liquid-filling auxiliary device with the dynamic testing system.

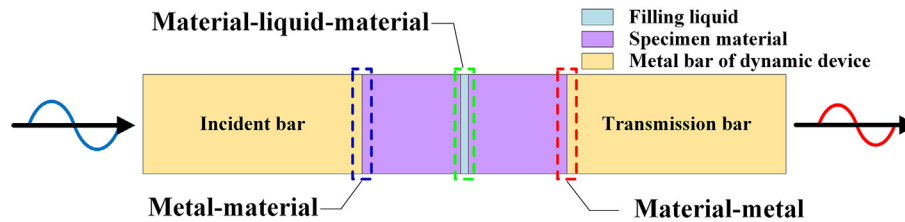


Fig. 7. Effect of diverse contact surfaces on the energy attenuation coefficient in the dynamic test process.

surfaces. For the term $\Delta E_{n, \text{metal-material}}$, a correction value of 0.191 was applied to the energy propagation coefficient for the granite specimens, while 0.363 was chosen as the coefficient for the PMMA specimens according to the published literature and due to the use of identical dynamic loading test conditions and contact surfaces between the metal bars and specimen in previous research (Huang et al., 2020). The result analysis of energy propagation coefficients, simply defined as E_n for the subsequent section in this paper, was based on data from a correction test.

3.1.2. Peak liquid pressure

The in situ hydraulic–mechanical balance is disturbed when a water-bearing fault is subjected to dynamic loading. Pressure analysis of the filling liquid is essential for investigating the effective stress of the surrounding rock and the stability of support structures in underground construction projects. The peak liquid pressure p_e , which is defined as the maximum pressure measured during the entire dynamic loading process in the laboratory investigation, was used to depict the response features of the filling liquid at the liquid-filled rock joints under dynamic conditions. The pressure signals were collected from the dynamic sensor in the metallic cavity with an initial voltage form, and sensor conversion parameters were applied to obtain pressure information.

A representative pressure–time curve for the filling liquid in one liquid-filled rock joint in a granite specimen with the joint inclination of 0° is illustrated as an example in Fig. 8, and this is further investigated along with the internal mechanisms of this system in the following section. Fig. 8 revealed that: (i) the acquisition time of data collected by the dynamic sensor was 0.02 s, and the liquid pressure change mainly occurred between 0 s and 0.01 s; (ii) the initial change in the liquid pressure lagged slightly behind the initial change in the strain signal of the incident bar (by approximately 0.001 s), which usually occurred for initial changes in signals of the incident and transmission bars; (iii) the pressure of the filling liquid exhibited frequent fluctuations and multiple extreme values, as indicated by the colored bars, and then decayed to a relatively stable level (0 MPa); and (iv) the extreme value of the

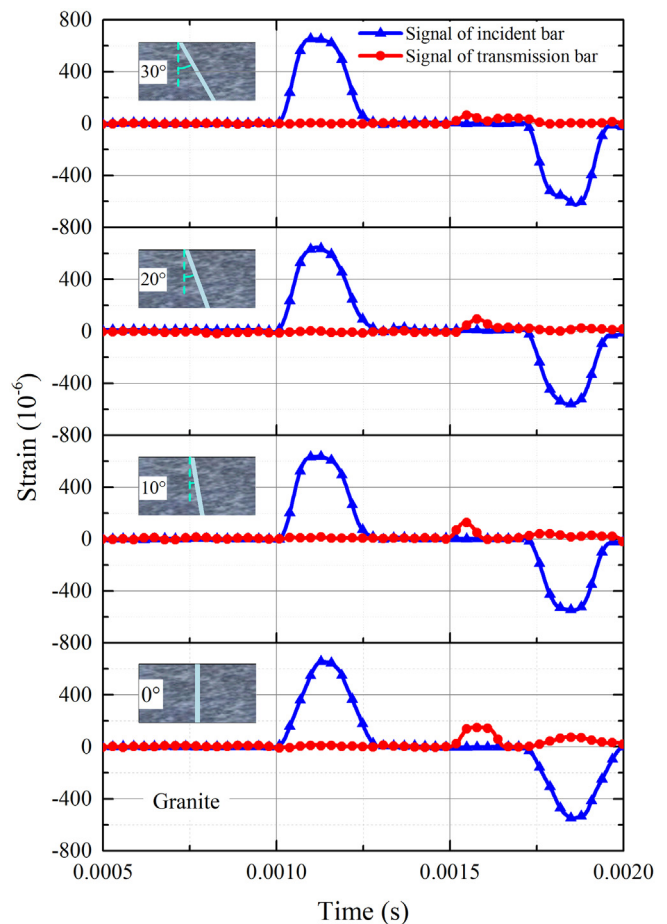


Fig. 9. Comparison of typical strain–time curves of granite specimens under different joint inclinations.

pressure change exhibited a relatively uniform trend of initially increasing gradually before decreasing, and the peak liquid pressure often exhibited a second or subsequent extreme value with a magnitude between 3 MPa and 5 MPa.

3.2. Energy propagation and attenuation of waves propagating across liquid-filled rock joints under dynamic loading

Comparisons of typical strain–time curves of granite and PMMA specimens with different joint inclinations are shown in Figs. 9 and 10, respectively. The signals acquired from the strain gauges on the incident and transmission bars are represented by the blue and red lines, respectively. The data in the initial period (0–0.002 s), which included the first waveform signals recorded on the incident and transmission bars, were selected for further analysis of wave energy propagation and attenuation. Overall, the waveforms and

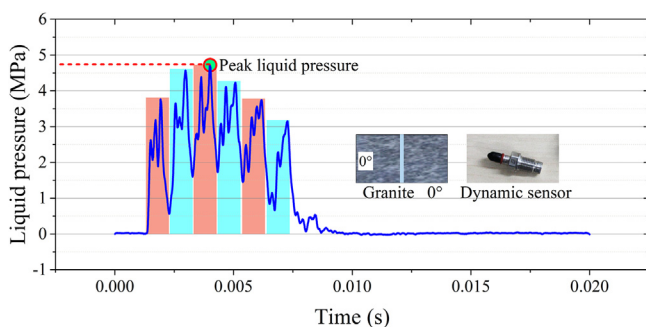


Fig. 8. Typical liquid pressure–time curve measured for liquid-filled rock joints of granite specimens with inclinations of 0° .

intensities of the signals from the incident bar remained consistent, primarily because of the consistent dynamic loading conditions, whereas the signals from the transmission bar changed with variations in the joint inclinations of liquid-filled joints. The amplitudes of the transmission bar signals decreased gradually as the orientation of the testing joints increased under certain experimental conditions, and smaller transmission signals were obtained for granite than for the PMMA under the same dynamic testing conditions. Specifically, when the joint orientation changed from 0° to 30° at intervals of 10° , which is the acute angle between the impact loading direction and the normal direction of the joint surface, the energy propagation coefficient varied as 0.416, 0.392, 0.341, and 0.293 for the granite specimens and 0.612, 0.593, 0.534, and 0.492 for the PMMA specimens, respectively. The results of all tests for specimens with varying joint inclinations are summarized in Table 2.

The overall trend for variation of the energy propagation coefficient with respect to joint orientation was consistent with the tendency noted from laboratory observations of waves propagating through joint specimens by Li et al. (2019a) and Yu et al. (2020). Within the range of tested joint angles from 0° to 30° , the variation in the energy propagation coefficient induced by the dynamic loading was not obvious, and there was a slight decrease from 0.416 to 0.293 for granite and from 0.612 to 0.492 for PMMA. These results indicate that larger joint inclinations correspond to greater energy attenuation for a given joint angle range, as shown in Fig. 11. The wave impedance of the medium, which is usually taken to be the product of the wave velocity and density, is critical in wave propagation characteristics and can cause attenuation in geophysics and rock dynamics. Large differences in the impedances of adjacent layers lead to energy attenuation, which in turn leads to

poor transmission of stress waves. For the liquid-filled rock joints considered in this study, the difference in the wave resistance of granite and water was larger than that of PMMA and water, which resulted in greater energy attenuation when the waves crossed the interface between granite and filling liquid. This phenomenon may account for the relatively small value obtained for the energy propagation coefficient of granite compared to that of PMMA under certain experimental conditions, and similar observations were made in a previous study (Huang et al., 2020). Apart from that, the better isotropy and homogeneity of PMMA, together with its fewer internal cracks and defects which could cause interference of wave signal propagation, it could be another possible explanation for greater value of energy propagation coefficient for PMMA to some extent.

For stress wave propagation across joints with diverse inclinations, which can be regarded as a problem for oblique incident cases of waves, the investigation is further complicated by the complex wave transformations and alternation of these waves compared with normal incident scenarios (Li and Ma, 2010; Zou et al., 2019). It is difficult to conducting laboratory tests on oblique incident waves through joints, especially for filled joints. In this study, an energy propagation coefficient was determined to analyze the energy attenuation and transmission of stress waves induced by dynamic impact loading. This process involves several factors previously mentioned in the theoretical derivation of this phenomenon, such as the waveform transformation, joint stiffness, and other parameters, owing to the limitations of current testing conditions. The coefficient introduced in this study differs slightly from the transmission coefficient typically used in theoretical analyses, which is defined as the ratio of the energy of transmission wave to that of the incident wave based on a rigorous definition from a mathematical perspective. It may aid in comprehensively describing the characteristics of energy changes for wave propagation through liquid-filled rock joints. The waves generated by the impact of the striker bar in the SHPB have larger amplitudes and lower frequencies than waves induced by ultrasonic devices, since the former waves are considered to be mainly composed of longitudinal waves for simplicity in this study. For wave propagation across rock joints with diverse inclinations based on a theoretical analysis, the energy of the transmission wave was mainly constrained in the transmission wave of the same type as the incident wave propagating through the joint (Zhu and Zhao, 2013). In addition, the transverse wave cannot propagate in the filling liquid owing to the lack of shear elasticity; therefore, the coefficient variation for cases involving transmitted longitudinal waves that correspond to the incidence of longitudinal waves was selected and analyzed. Specifically, considering previous findings regarding interactions between waves and joints, the transmission coefficients obtained by mathematical analyses for transmitted longitudinal waves decrease with incident longitudinal waves within the range 0° – 30° in nonlinear joint models (Liu et al., 2020b), which is similar to the results observed in this study. In addition, the transmission coefficient does not change significantly (Gu et al., 1996; Li et al., 2018a) and remains nearly constant with the joint inclination until it is approximately perpendicular to the joint (Li et al., 2014). The discrepancy in the variation trend may be attributed to the simplified joint and wave properties used in the above analysis, including the ideal medium assumption and simplified incident waveform. The wave signal obtained in laboratory experiments did not focus directly on the adjacent zone of the joint, which may differ from the theoretical analysis. Further work is required to completely interpret the relationship between the energy propagation coefficient for liquid-filled rock joints and variations of the joint inclination based on experimental tests.

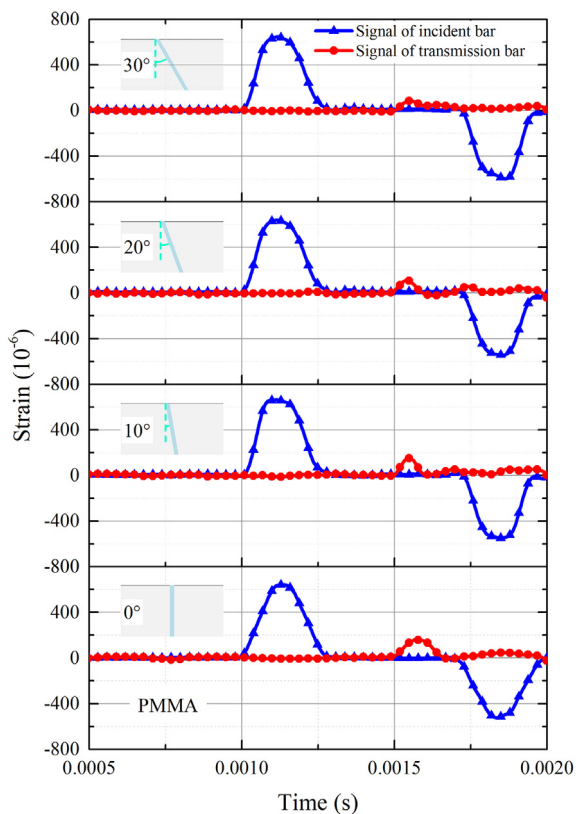


Fig. 10. Comparison of typical strain-time curves of PMMA specimens under different joint inclinations.

Table 2
Results of dynamic tests of all specimens with different joint inclinations.

Joint inclination (°)	Granite					PMMA				
	No.	$\varepsilon_i (10^{-6})$	$\varepsilon_t (10^{-6})$	E_n	p_e (MPa)	No.	$\varepsilon_i (10^{-6})$	$\varepsilon_t (10^{-6})$	E_n	p_e (MPa)
0	G0-1	641.25	144.92	0.417	4.73	P0-1	642.18	161.19	0.614	4.09
	G0-2	639.79	142.03	0.413	4.68	P0-2	643.29	160.82	0.613	4.1
	G0-3	640.17	145.32	0.418	4.7	P0-3	638.71	159.04	0.612	4.06
	G0-4	642.10	142.55	0.413	4.74	P0-4	639.23	158.53	0.611	4.08
	G0-5	640.25	143.42	0.415	4.7	P0-5	640.35	157.53	0.609	4.08
	G0-6	641.78	146.97	0.42	4.71	P0-6	641.35	160.34	0.613	4.07
	Average			0.416	4.71	Average			0.612	4.08
10	G10-1	640.18	126.76	0.389	4.61	P10-1	642.17	148.34	0.594	3.92
	G10-2	642.16	129.07	0.392	4.62	P10-2	639.79	145.23	0.59	3.85
	G10-3	640.41	127.44	0.39	4.61	P10-3	642.15	145.13	0.589	3.89
	G10-4	641.25	126.33	0.388	4.6	P10-4	640.25	148.54	0.595	3.9
	G10-5	639.72	130.5	0.395	4.59	P10-5	641.17	146.19	0.591	3.88
	G10-6	640.05	132.49	0.398	4.59	P10-6	640.73	151.21	0.599	3.9
	Average			0.392	4.6	Average			0.593	3.89
20	G20-1	637.54	96.27	0.342	4.21	P20-1	640.17	108.83	0.533	3.63
	G20-2	641.29	95.55	0.34	4.26	P20-2	639.95	110.07	0.535	3.64
	G20-3	638.17	95.73	0.341	4.24	P20-3	639.21	106.75	0.53	3.62
	G20-4	636.75	94.24	0.339	4.22	P20-4	641.23	111.57	0.537	3.66
	G20-5	632.94	97.47	0.345	4.2	P20-5	640.72	107.64	0.531	3.64
	G20-6	640.63	94.81	0.339	4.25	P20-6	640.45	112.08	0.538	3.65
	Average			0.341	4.23	Average			0.534	3.64
30	G30-1	641.72	66.74	0.295	3.5	P30-1	636.71	81.5	0.491	3
	G30-2	638.79	63.24	0.29	3.49	P30-2	637.95	82.3	0.492	3.04
	G30-3	642.16	66.14	0.294	3.53	P30-3	638.12	82.32	0.492	3.03
	G30-4	640.59	62.78	0.289	3.51	P30-4	639.57	83.14	0.493	3.04
	G30-5	640.17	64.66	0.292	3.51	P30-5	635.29	80.05	0.489	2.99
	G30-6	641.91	68.68	0.298	3.52	P30-6	638.71	84.31	0.495	3.02
	Average			0.293	3.51	Average			0.492	3.02

Note: The granite and PMMA specimens were labeled GX-1 to GX-6 and PX-1 to PX-6, respectively, where X represents the different joint inclinations.

3.3. Dynamic response features of the filling liquid of liquid-filled rock joints with varied joint inclinations

As illustrated in Figs. 12 and 13, the liquid pressure values exhibited obvious fluctuations throughout the experiments involving impact loading of the granite and PMMA specimens, respectively. A dynamic sensor mounted on the metallic cavity of an auxiliary device used for producing filled joints was used to capture real-time data describing variations of the filling liquid. Investigations of the dynamic responses of the filling fluid in rock joints are of great importance for fundamental research on engineering practices involving geophysics and rock dynamics. Different inclinations were obtained by adjusting the angle between the normal direction of the joint surface and the impact loading direction, and the same thicknesses were achieved by controlling the apertures of the sandwiched artificial joints. The thickness was set to 3 mm due to commissioning of the equipment installation to ensure test results. From Figs. 12 and 13, we observe that the fluctuations in liquid pressure lasted for 0.01–0.015 s, the peak values of the liquid pressure varied with different joint inclinations, and the peak liquid pressure of granite was slightly greater than that of PMMA. Concretely speaking, for the liquid-filled rock joints described in this paper, the peak liquid pressure varied and showed values of 4.71 MPa, 4.6 MPa, 4.23 MPa and 3.51 MPa for granite, and the corresponding values were 4.08 MPa, 3.89 MPa, 3.64 MPa and 3.02 MPa for PMMA.

The variation curves for liquid pressure were obtained under impact loading, and the obtained peak values were used to characterize the dynamic response of the liquid. To further investigate the effects of joint inclination in liquid-filled rock joints on the characteristics of the filling liquid, the variations in peak liquid pressures were compared for the two different materials, as shown in Fig. 14. In this study, PMMA specimens with the same geometry and size were prepared to obtain reference

data because their homogeneity and isotropy were better than those of granite. As determined by trial and error, the gas pressure for the striker bar of the dynamic loading device was set at 0.35 MPa. This was used to ensure that the simulation materials of the rock matrix did not undergo failure and were in an elastic state. The occurrence of severe fragmentation in the current study could cause leakage of the filling liquid and affect the monitoring of the liquid pressure. Further analyses considering the dynamic responses of these systems to fragmentation will be conducted in the future.

For different joint inclinations in this study, we discovered a decreasing trend for peak liquid pressure with respect to joint orientation for both test materials. To be specific, the value varied from 4.71 MPa to 3.51 MPa for granite and from 4.08 MPa to 3.02 MPa for PMMA. This indicates that less energy was obtained by the filling liquid from dynamic impact loading at larger inclinations. It should be noted that the spatial distribution of the filling fluid in the joint is affected by the joint inclination, which was observed in a previous study of the interactions between waves and oblique filled joints (Yang et al., 2020). As illustrated in Fig. 15, force analysis of the liquid-filled rock joints under loading was carried out. Fig. 15a shows a schematic for the stress analysis of a component of the inclined specimen and filling liquid layer in the axial direction. The stress decomposition of the liquid-filling layer is shown in Fig. 15b.

The following assumptions were made in the subsequent analysis: (i) stress equilibrium exists between the sides of the specimen with an oblique plane and liquid-filling layer when subjected to dynamic loading in the testing process, as shown in Eq. (5); and (ii) normal stress changes the volume of the unit body element, which is considered to be the smallest unit in the fluid, while the shear stress changes the shape of the unit body but does not change its volume according to fluid mechanics. These assumptions can be described by the following equations:

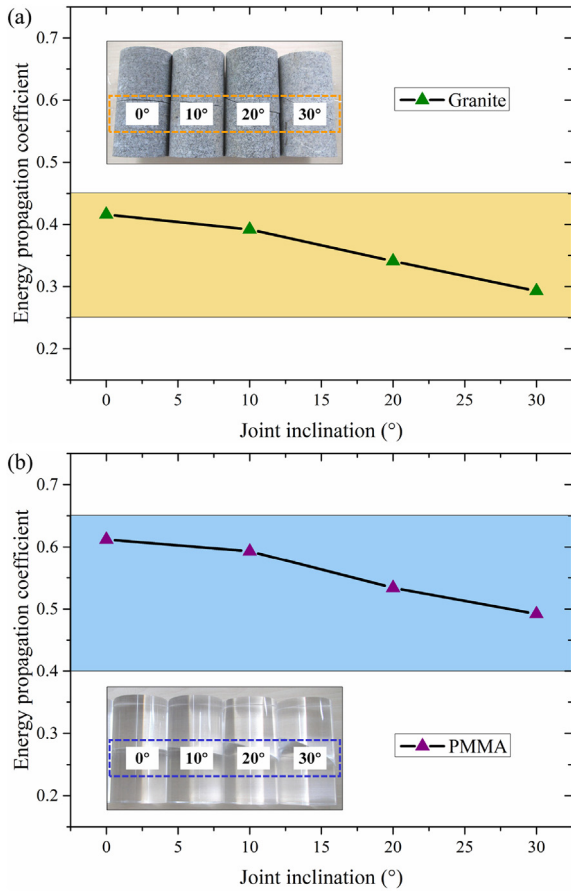


Fig. 11. Relationship between the energy propagation coefficient and the joint inclination of experimental specimens: (a) Granite, and (b) PMMA.

$$F_0 = p_0 A_0 = p_\theta A_\theta \quad (5)$$

$$A_0 = A_\theta \cos \theta \quad (6)$$

$$p_\theta = p_1 \quad (7)$$

$$p_1 = p'_1 \quad (8)$$

$$p_{11} = p_1 \cos \theta = p'_1 \cos \theta = p'_{11} \quad (9)$$

$$p_{12} = p_1 \sin \theta = p'_1 \sin \theta = p'_{12} \quad (10)$$

where the normal stress p_0 acts on the leftmost face of the specimen, and the results of these stresses are described by the force F_0 , which is considered to be constant because the initial impact conditions are controlled by setting the gas pressure at a fixed value. θ denotes the joint inclination of the specimens. The stresses acting on the oblique section are represented by p_θ , and the corresponding force is F_θ . A_0 and A_θ denote the entire and inclined section areas, respectively. Based on Newton's third law, we know that the filling liquid exerts a force of equal magnitude in the opposite direction onto the surface, which is denoted by p_1 , and the stresses acting on the other side of the liquid layer are described by p'_1 . p_{11} and p'_{11} represent the normal stress caused by the action of the filling liquid, which is perpendicular to the inclined plane, and

p_{12} and p'_{12} are the shear stress caused by the action of the filling liquid, which are tangential to the inclined plane.

By combining Eq. (5)–(10), the normal and shear stresses acting on the filling liquid layer are expressed by the following equations:

$$p_{11} = p_0 \cos^2 \theta \quad (11)$$

$$p_{12} = p_0 \sin \theta \cos \theta \quad (12)$$

Based on the above assumptions, the shear stress component does not change the volume of the unit body element under the given conditions, and the liquid pressure may be mainly controlled by p_{11} . The term p_0 in Eq. (11) may be considered to be a constant, indicating that the joint inclination is an important parameter for the range of angles considered in this study. The peak liquid pressure of the filling liquid during impact loading is related to the pressure variation, which is affected by the joint inclination. It was noted that the value of p_{11} decreased with increasing joint angle, as determined by Eq. (11). The variations observed in the above analysis are similar to those observed experimentally, as shown in Fig. 14. In addition, the total energy induced by the incident bar was assumed to be constant under the given loading conditions. Considering the relationship between joint orientation and energy propagation coefficient, less input energy may be transmitted through the rock material, and the remaining energy will act on the filling liquid layer, which might explain why the peak liquid pressure of granite was slightly greater than that of PMMA. These results suggest that the joint inclination could make the liquid-filling layer in liquid-filled rock joints more prone to considerable changes and increase the probability of rock fragmentation and failure. These phenomena are related to the hydraulic-dynamic hazards associated with underground rock structures and provide considerable theoretical significance and value for engineering applications.

This study was mainly focused on investigating the response characteristics of a single liquid-filled rock joint with different joint orientations under dynamic impact conditions. However, the influences of environmental parameters, the number of joints, and lithology should also be further investigated to better understand the interactions involved in these systems. For instance, it has been

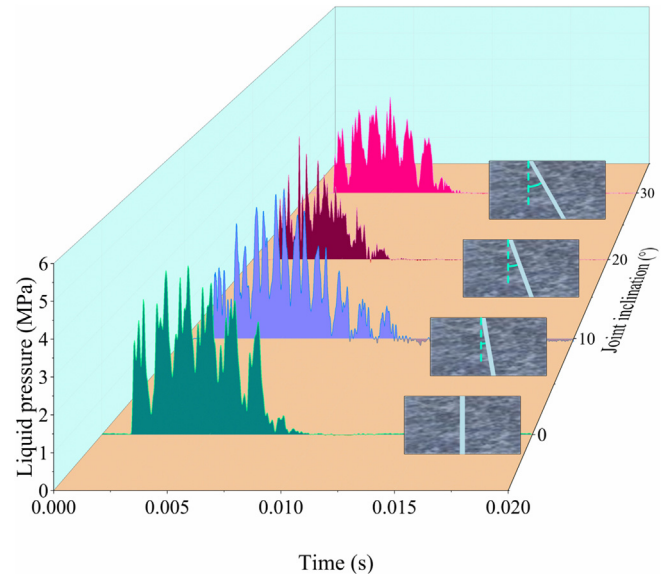


Fig. 12. Comparison of typical liquid pressure-time curves for granite specimens with different joint inclinations.

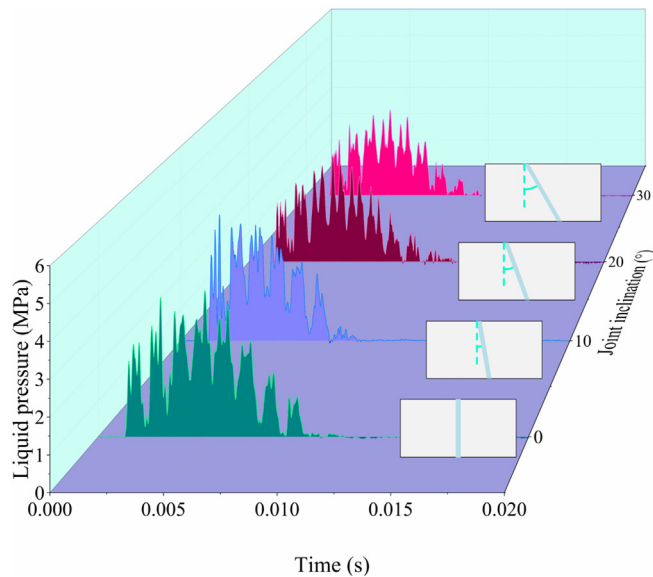


Fig. 13. Comparison of typical liquid pressure-time curves for PMMA specimens with different joint inclinations.

shown that multiple joint sets with various numbers of joints affect the seismic features of rock masses (Zhao et al., 2006; Li et al., 2012). Additionally, thermal effects should be considered in studies of rock joint behavior in underground rock engineering projects (Yang et al., 2021). Therefore, investigations of additional influencing factors via laboratory or field tests for liquid-filled rock joints should be conducted in future studies. Furthermore, numerical and theoretical analyses should be carried out to obtain improved verification and validation of the experimental observations to fully reveal the mechanisms for interactions between stress waves and liquid-filled rock joints.

4. Conclusions

Characterizing and understanding the dynamic behavior of liquid-filled rock joints under large impact loadings is essential for the design and safety of underground rock engineering projects. In

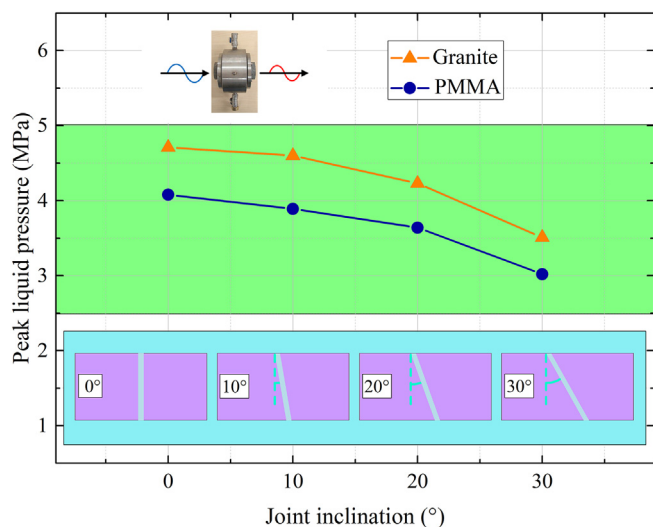


Fig. 14. Relationships between peak liquid pressure and joint inclination for granite and PMMA specimens.

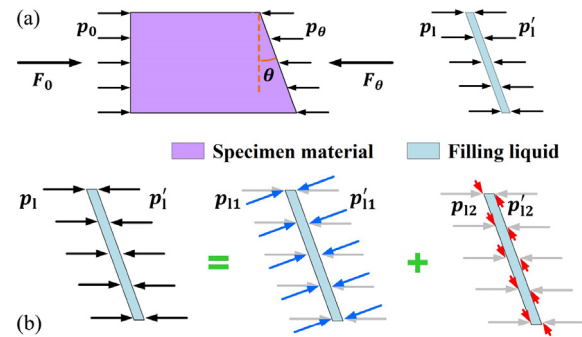


Fig. 15. Diagrammatic sketch of the force analysis for liquid-filled rock joints under dynamic loading: (a) Specimen and filling liquid (axial direction), and (b) Stress decomposition for filling liquid.

this study, a series of dynamic impact loading tests was conducted on liquid-filled rock joints that were modeled using granite and PMMA materials using liquid-filling auxiliary device and SHPB. Based on the results of laboratory-scale investigations, the main conclusions are as follows:

- (1) A liquid-filling auxiliary device can be utilized to model liquid-filled rock joints to investigate their effects on response characteristics with diverse joint orientations under dynamic loading conditions.
- (2) The energy propagation coefficient is proposed to depict the energy behavior of waves propagating across liquid-filled rock joints, which gently diminishes with increasing joint inclinations, and smaller values of the energy propagation coefficient were obtained for granite than that for PMMA under given experimental conditions.
- (3) The dynamic response features of the filling liquid in the liquid-filled rock joints are described by the peak liquid pressure, which gradually decreases with increasing joint orientation, and the peak liquid pressure in granite is slightly greater than that in PMMA under certain test angle.
- (4) The results of this research might provide a considerable method to better study liquid-filled rock joints at the laboratory scale, and the findings in the present study could serve as guidance for interpreting and analyzing the coupling of hydraulic-dynamic hazards of underground rock engineering.

Declaration of competing interest

The authors declare that they have no known competing financial interests or personal relationships that could have appeared to influence the work reported in this paper.

Acknowledgments

This work was financially supported by the National Key Research and Development Plan of China (Grant No. 2018YFC1504902), the National Natural Science Foundation of China (Grant No. 52079068) and the State Key Laboratory of Hydrosience and Engineering, China (Grant No. 2021-KY-04).

References

- Barton, N.R., 2002. Some new q-value correlations to assist in site characterization and tunnel design. *Int. J. Rock Mech. Min. Sci.* 39 (2), 185–216.
- Berkowitz, B., 2002. Characterizing flow and transport in fractured geological media: a review. *Adv. Water Resour.* 25 (8–12), 861–884.

- Chen, Y.F., Liao, Z., Zhou, J.Q., Hu, R., Yang, Z.B., Zhao, X.J., Wu, X.L., Yang, X.L., 2020. Non-Darcian flow effect on discharge into a tunnel in karst aquifers. *Int. J. Rock Mech. Min. Sci.* 130, 104319.
- Cook, N.G.W., 1992. Natural joints in rock: mechanical, hydraulic and seismic behaviour and properties under normal stress. *Int. J. Rock Mech. Min. Sci. Geomech. Abstr.* 29 (3), 198–223.
- Dai, F., Huang, S., Xia, K.W., Tan, Z.Y., 2010. Some fundamental issues in dynamic compression and tension tests of rocks using split Hopkinson pressure bar. *Rock Mech. Rock Eng.* 43 (6), 657–666.
- Dai, F., Xu, Y., Zhao, T., Xu, N.W., Liu, Y., 2016. Loading-rate-dependent progressive fracturing of cracked chevron-notched Brazilian disc specimens in split Hopkinson pressure bar tests. *Int. J. Rock Mech. Min. Sci.* 88, 49–60.
- Fan, L.F., Wu, Z.J., Wan, Z., Gao, J.W., 2017. Experimental investigation of thermal effects on dynamic behavior of granite. *Appl. Therm. Eng.* 125, 94–103.
- Field, J.E., Walley, S.M., Proud, W.G., Goldrein, H.T., Siviour, C.R., 2004. Review of experimental techniques for high rate deformation and shock studies. *Int. J. Impact Eng.* 30 (7), 725–775.
- Flores, R.M., 1998. Coalbed methane: from hazard to resource. *Int. J. Coal Geol.* 35 (1–4), 3–26.
- Frew, D.J., Forrestal, M.J., Chen, W., 2001. A split Hopkinson pressure bar technique to determine compressive stress–strain data for rock materials. *Exp. Mech.* 41 (1), 40–46.
- Goldsmith, W., Sackman, J.L., Ewerts, C., 1976. Static and dynamic fracture strength of Barre granite. *Int. J. Rock Mech. Min. Sci. Geomech. Abstr.* 13 (11), 303–309.
- Gu, B.L., Suárez-Rivera, R., Nihei, K.T., Myer, L.R., 1996. Incidence of plane waves upon a fracture. *J. Geophys. Res. B Solid Earth* 101 (B11), 25337–25346.
- Hajiabdomajid, V., Kaiser, P., 2003. Brittleness of rock and stability assessment in hard rock tunneling. *Tunn. Undergr. Space Technol.* 18 (1), 35–48.
- Han, G.F., Liu, X.L., Huang, J., Nawit, K., Sun, L., 2020a. Modified Boltzmann equation and extended Navier-Stokes equations. *Phys. Fluids* 32 (2), 022001.
- Han, Z.Y., Li, D.Y., Zhou, T., Zhu, Q.Q., Ranjith, P.G., 2020b. Experimental study of stress wave propagation and energy characteristics across rock specimens containing cemented mortar joint with various thicknesses. *Int. J. Rock Mech. Min. Sci.* 131, 104352.
- Hopkinson, J., 1872. On the rupture of iron wire by a blow. In: *Proceedings of Literary and Philosophical Society of Manchester*, 1, pp. 40–45.
- Hopkinson, B.X., 1914. A method of measuring the pressure produced in the detonation of high explosives or by the impact of bullets. In: *Philosophical Transactions of the Royal Society of London. Series A, Containing Papers of a Mathematical or Physical Character*, 213, pp. 437–456, 497–508.
- Howe, S.P., Goldsmith, W., Sackman, J.L., 1974. Macroscopic static and dynamic mechanical properties of Yule marble. *Exp. Mech.* 14 (9), 337–346.
- Huang, X.L., Qi, S.W., Xia, K.W., Zheng, H., Zheng, B.W., 2016. Propagation of high amplitude stress waves through a filled artificial joint: an experimental study. *J. Appl. Geophys.* 130, 1–7.
- Huang, J., Liu, X.L., Zhao, J., Wang, E.Z., Wang, S.J., 2020. Propagation of stress waves through fully saturated rock joint under undrained conditions and dynamic response characteristics of filling liquid. *Rock Mech. Rock Eng.* 53 (8), 3637–3655.
- Jiang, S., Shen, L.M., Guillard, F., Einav, I., 2021. The effect of cement material properties on the fracture patterns developing within cement-covered brittle sphere under impact. *Acta Geotech.* 16 (3), 763–773.
- Ju, Y., Sudak, L., Xie, H.P., 2007. Study on stress wave propagation in fractured rocks with fractal joint surfaces. *Int. J. Solid Struct.* 44 (13), 4256–4271.
- Klepaczko, J.R., Bassim, M.N., Hsu, T.R., 1984. Fracture toughness of coal under quasi-static and impact loading. *Eng. Fract. Mech.* 19 (2), 305–316.
- Kolsky, H., 1949. An investigation of the mechanical properties of materials at very high rates of loading. *Proc. Phys. Soc. B* 62 (11), 676–700.
- Li, X.B., Lok, T.S., Zhao, J., 2005. Dynamic characteristics of granite subjected to intermediate loading rate. *Rock Mech. Rock Eng.* 38 (1), 21–39.
- Li, X.Z., Hua, A.Z., 2006. Prediction and prevention of sandstone-gas outbursts in coal mines. *Int. J. Rock Mech. Min. Sci.* 43 (1), 2–18.
- Li, X.B., Zhou, Z.L., Zhao, F.J., Zuo, Y.J., Ma, C.D., Ye, Z.Y., Hong, L., 2009. Mechanical properties of rock under coupled static-dynamic loads. *J. Rock Mech. Geotech. Eng.* 1 (1), 41–47.
- Li, J.C., Ma, G.W., 2010. Analysis of blast wave interaction with a rock joint. *Rock Mech. Rock Eng.* 43 (6), 777–787.
- Li, J.C., Ma, G.W., Zhao, J., 2011. Stress wave interaction with a nonlinear and slippery rock joint. *Int. J. Rock Mech. Min. Sci.* 48 (3), 493–500.
- Li, J.C., Li, H.B., Ma, G.W., Zhao, J., 2012. A time-domain recursive method to analyse transient wave propagation across rock joints. *Geophys. J. Int.* 188 (2), 631–644.
- Li, S.C., Zhou, Z.Q., Li, L.P., Xu, Z.H., Zhang, Q.Q., Shi, S.S., 2013. Risk assessment of water inrush in karst tunnels based on attribute synthetic evaluation system. *Tunn. Undergr. Space Technol.* 38, 50–58.
- Li, J.C., Li, H.B., Jiao, Y.Y., Liu, Y.Q., Xia, X., Yu, C., 2014. Analysis for oblique wave propagation across filled joints based on thin-layer interface model. *J. Appl. Geophys.* 102, 39–46.
- Li, S.C., Liu, R.T., Zhang, Q.S., Zhang, X., 2016a. Protection against water or mud inrush in tunnels by grouting: a review. *J. Rock Mech. Geotech. Eng.* 8 (5), 753–766.
- Li, S.C., Zhou, Z.Q., Li, L.P., Lin, P., Xu, Z.H., Shi, S.S., 2016b. A new quantitative method for risk assessment of geological disasters in underground engineering: attribute Interval Evaluation Theory (AIET). *Tunn. Undergr. Space Technol.* 53, 128–139.
- Li, X.F., Li, H.B., Li, J.C., Li, Z.W., 2018a. Research on transient wave propagation across nonlinear joints filled with granular materials. *Rock Mech. Rock Eng.* 51 (8), 2373–2393.
- Li, X.F., Li, X., Li, H.B., Zhang, Q.B., Zhao, J., 2018b. Dynamic tensile behaviours of heterogeneous rocks: the grain scale fracturing characteristics on strength and fragmentation. *Int. J. Impact Eng.* 118, 98–118.
- Li, D.Y., Han, Z.Y., Zhu, Q.Q., Zhang, Y., Ranjith, P.G., 2019a. Stress wave propagation and dynamic behavior of red sandstone with single bonded planar joint at various angles. *Int. J. Rock Mech. Min. Sci.* 117, 162–170.
- Li, J.C., Rong, L.F., Li, H.B., Hong, S.N., 2019b. An SHPB test study on stress wave energy attenuation in jointed rock masses. *Rock Mech. Rock Eng.* 52 (2), 403–420.
- Li, L.P., Sun, S.Q., Wang, J., Yang, W.W., Song, S.G., Fang, Z.D., 2020. Experimental study of the precursor information of the water inrush in shield tunnels due to the proximity of a water-filled cave. *Int. J. Rock Mech. Min. Sci.* 130, 104320.
- Liu, X.L., Wang, S.J., Wang, S.Y., Wang, E.Z., 2015. Fluid-driven fractures in granular materials. *Bull. Eng. Geol. Environ.* 74 (2), 621–636.
- Liu, X.L., Han, G.F., Wang, E.Z., Wang, S.J., Nawit, K., 2018. Multiscale hierarchical analysis of rock mass and prediction of its mechanical and hydraulic properties. *J. Rock Mech. Geotech. Eng.* 10 (4), 694–702.
- Liu, X.L., Wang, F., Huang, J., Wang, S.J., Zhang, Z.Z., Nawit, K., 2019. Grout diffusion in silty fine sand stratum with high groundwater level for tunnel construction. *Tunn. Undergr. Space Technol.* 93, 103051.
- Liu, Q.S., Wu, J., Zhang, X.P., Tang, L.X., Bi, C., Li, W.W., Xu, J.L., 2020a. Microseismic monitoring to characterize structure-type rockbursts: a case study of a TBM-excavated tunnel. *Rock Mech. Rock Eng.* 53 (7), 2995–3013.
- Liu, T.T., Li, X.P., Zheng, Y., Meng, F., Song, D.R., 2020b. Analysis of seismic waves propagating through an in situ stressed rock mass using a nonlinear model. *Int. J. Geomech.* 20 (3), 04020002.
- Ma, H.S., Yin, L.J., Gong, Q.M., Wang, J., 2015. TBM tunneling in mixed-face ground: problems and solutions. *Int. J. Min. Sci. Technol.* 25 (4), 641–647.
- Ma, T.H., Tang, C.A., Tang, S.B., Kuang, L., Yu, Q., Kong, D.Q., Zhu, X., 2018. Rockburst mechanism and prediction based on microseismic monitoring. *Int. J. Rock Mech. Min. Sci.* 110, 177–188.
- Ma, L.J., Wu, J.W., Wang, M.Y., Dong, L., Wei, H.Z., 2020. Dynamic compressive properties of dry and saturated coral rocks at high strain rates. *Eng. Geol.* 272, 105615.
- Manouchehrian, A., Cai, M., 2017. Analysis of rockburst in tunnels subjected to static and dynamic loads. *J. Rock Mech. Geotech. Eng.* 9 (6), 1031–1040.
- Martino, J.B., Chandler, N.A., 2004. Excavation-induced damage studies at the underground research laboratory. *Int. J. Rock Mech. Min. Sci.* 41 (8), 1413–1426.
- Ortlepp, W.D., Stacey, T.R., 1994. Rockburst mechanisms in tunnels and shafts. *Tunn. Undergr. Space Technol.* 9 (1), 59–65.
- Pei, P.D., Dai, F., Liu, Y., Wei, M.D., 2020. Dynamic tensile behavior of rocks under static pre-tension using the flattened Brazilian disc method. *Int. J. Rock Mech. Min. Sci.* 126, 104208.
- Perkins, R.D., Green, S.J., Friedman, M., 1970. Uniaxial stress behavior of porphyritic tonalite at strain rates to 103/second. *Int. J. Rock Mech. Min. Sci. Geomech. Abstr.* 7 (5), 527–535.
- Pyrak-Nolte, L.J., Myer, L.R., Cook, N.G.W., 1990. Transmission of seismic waves across single natural fractures. *J. Geophys. Res.* 95 (B6), 8617–8638.
- Qian, Q.H., Zhou, X.P., 2018. Failure behaviors and rock deformation during excavation of Underground Cavern Group for Jinping I hydropower station. *Rock Mech. Rock Eng.* 51 (8), 2639–2651.
- Si, X.F., Gong, F.Q., Li, X.B., Wang, S.Y., Luo, S., 2019. Dynamic Mohr–Coulomb and Hoek–Brown strength criteria of sandstone at high strain rates. *Int. J. Rock Mech. Min. Sci.* 115, 48–59.
- Sun, H., Liu, X.L., Zhu, J.B., 2019. Correlational fractal characterisation of stress and acoustic emission during coal and rock failure under multilevel dynamic loading. *Int. J. Rock Mech. Min. Sci.* 117, 1–10.
- Wang, X.M., Zhu, Z.M., Wang, M., Ying, P., Zhou, L., Dong, Y.Q., 2017. Study of rock dynamic fracture toughness by using VB-SCSC specimens under medium-low speed impacts. *Eng. Fract. Mech.* 181, 52–64.
- Wang, Q., Jiang, B., Pan, R., Li, S.C., He, M.C., Sun, H.B., Qin, Q., Yu, H.C., Luan, Y.C., 2018. Failure mechanism of surrounding rock with high stress and confined concrete support system. *Int. J. Rock Mech. Min. Sci.* 102, 89–100.
- Watanabe, I., Ueno, S., Koga, M., Muramoto, K., Abe, T., Goto, T., 1992. Safety and disaster prevention measures for underground space: an analysis of disaster cases. *Tunn. Undergr. Space Technol.* 7 (4), 317–324.
- Watanabe, T., Sassa, K., 1995. Velocity and amplitude of P-waves transmitted through fracture zones composed of multiple thin low-velocity layers. *Int. J. Rock Mech. Min. Sci. Geomech. Abstr.* 32 (4), 313–324.
- Wei, X.F., Liu, X.L., Duan, Y.L., Feng, J.M., 2017. Property transformation of a modified sulfoaluminate grouting material under pressure circulation for a water-sealed underground oil cavern. *Construct. Build. Mater.* 140, 210–220.
- Wen, S., Zhang, C.S., Chang, Y.L., Hu, P., 2020. Dynamic compression characteristics of layered rock mass of significant strength changes in adjacent layers. *J. Rock Mech. Geotech. Eng.* 12 (2), 353–365.
- Wu, W., Zhu, J.B., Zhao, J., 2013. Dynamic response of a rock fracture filled with viscoelastic materials. *Eng. Geol.* 160, 1–7.
- Wu, B.B., Yao, W., Xia, K.W., 2016. An experimental study of dynamic tensile failure of rocks subjected to hydrostatic confinement. *Rock Mech. Rock Eng.* 49 (10), 3855–3864.

- Xia, K.W., Nasser, M.H.B., Mohanty, B., Lu, F., Chen, R., Luo, S.N., 2008. Effects of microstructures on dynamic compression of Barre granite. *Int. J. Rock Mech. Min. Sci.* 45 (6), 879–887.
- Xia, K.W., Yao, W., 2015. Dynamic rock tests using split Hopkinson (Kolsky) bar system – a review. *J. Rock Mech. Geotech. Eng.* 7 (1), 27–59.
- Xiao, Y.X., Feng, X.T., Li, S.J., Feng, G.L., Yu, Y., 2016. Rock mass failure mechanisms during the evolution process of rockbursts in tunnels. *Int. J. Rock Mech. Min. Sci.* 83, 174–181.
- Yang, S.Q., Chen, M., Jing, H.W., Chen, K.F., Meng, B., 2017. A case study on large deformation failure mechanism of deep soft rock roadway in Xin'an coal mine. *China. Eng. Geol.* 217, 89–101.
- Yang, H., Duan, H.F., Zhu, J.B., 2019. Ultrasonic P-wave propagation through water-filled rock joint: an experimental investigation. *J. Appl. Geophys.* 169, 1–14.
- Yang, H., Duan, H.F., Zhu, J.B., 2020. Effects of filling fluid type and composition and joint orientation on acoustic wave propagation across individual fluid-filled rock joints. *Int. J. Rock Mech. Min. Sci.* 128, 104248.
- Yang, H., Duan, H.F., Zhu, J.B., 2021. Thermal effect on compressional wave propagation across fluid-filled rock joints. *Rock Mech. Rock Eng.* 54 (1), 455–462.
- Yu, J., Liu, Z.H., He, Z., Zhou, X.Q., Ye, J.B., 2020. Fluctuation characteristic test of oblique stress waves in infilled jointed rock and study of the analytic method. *Adv. Civ. Eng.* 2020, 1–12.
- Zhang, G.H., Jiao, Y.Y., Ma, C.X., Wang, H., Chen, L.B., Tang, Z.C., 2018. Alteration characteristics of granite contact zone and treatment measures for inrush hazards during tunnel construction – a case study. *Eng. Geol.* 235, 64–80.
- Zhao, J., Zhou, Y.X., Hefny, A.M., Cai, J.G., Chen, S.G., Li, H.B., Liu, J.F., Jain, M., Foo, S.T., Seah, C.C., 1999. Rock dynamics research related to cavern development for ammunition storage. *Tunn. Undergr. Space Technol.* 14 (4), 513–526.
- Zhao, J., Li, H.B., 2000. Experimental determination of dynamic tensile properties of a granite. *Int. J. Rock Mech. Min. Sci.* 37 (5), 861–866.
- Zhao, J., Cai, J.G., Zhao, X.B., Li, H.B., 2006. Experimental study of ultrasonic wave attenuation across parallel fractures. *Geomechanics Geoengin.* 1 (2), 87–103.
- Zhao, Y.X., Zhao, G.F., Jiang, Y.D., Elsworth, D., Huang, Y.Q., 2014. Effects of bedding on the dynamic indirect tensile strength of coal: laboratory experiments and numerical simulation. *Int. J. Coal Geol.* 132, 81–93.
- Zhao, Y., Bi, J., Zhou, X.P., 2020. Quantitative analysis of rockburst in the surrounding rock masses around deep tunnels. *Eng. Geol.* 273, 105669.
- Zhou, A.T., Zhang, M., Wang, K., Elsworth, D., Wang, J.W., Fan, L.P., 2020a. Airflow disturbance induced by coal mine outburst shock waves: a case study of a gas outburst disaster in China. *Int. J. Rock Mech. Min. Sci.* 128, 104262.
- Zhou, Z., Cai, X., Li, X., Cao, W., Du, X., 2020b. Dynamic response and energy evolution of sandstone under coupled static–dynamic compression: insights from experimental study into Deep Rock engineering applications. *Rock Mech. Rock Eng.* 53 (3), 1305–1331.
- Zhu, W.C., Li, Z.H., Zhu, L.K., Tang, C.A., 2010. Numerical simulation on rockburst of underground opening triggered by dynamic disturbance. *Tunn. Undergr. Space Technol.* 25 (5), 587–599.
- Zhu, J.B., Zhao, J., 2013. Obliquely incident wave propagation across rock joints with virtual wave source method. *J. Appl. Geophys.* 88, 23–30.
- Zhu, J.B., Bao, W.Y., Peng, Q., Deng, X.F., 2020. Influence of substrate properties and interfacial roughness on static and dynamic tensile behaviour of rock-shotcrete interface from macro and micro views. *Int. J. Rock Mech. Min. Sci.* 132, 104350.
- Zou, C.J., Wong, L.N.Y., Loo, J.J., Gan, B.S., 2016. Different mechanical and cracking behaviors of single-flawed brittle gypsum specimens under dynamic and quasi-static loadings. *Eng. Geol.* 201, 71–84.
- Zou, Y., Li, J.C., Zhao, J., 2019. A novel experimental method to investigate the seismic response of rock joints under obliquely incident wave. *Rock Mech. Rock Eng.* 52 (9), 3459–3466.



Xiaoli Liu obtained his BSc and MSc degrees from Liaoning Technical University, China in 2001 and 2004, respectively, and his PhD degree from Tsinghua University, China in 2009. He serves as associate dean for the School of Civil Engineering at Tsinghua University. He serves on the editorial boards of several renowned international journals, including *Tunneling and Underground Space Technology*, and *Environmental Geotechnics*. His research interests include geotechnical and geo-environmental engineering, thermo-hydro-mechanical and chemical (THMC) coupling mechanism in geological system, tunnel boring machine (TBM) tunneling technique and underground storage of energies and resources. He has authored/coauthored over 180 papers published in peer-reviewed scientific journals and conferences in these areas. He is active in academic activities and consultancies and has served as a member of many projects and conference committees. He obtained the National Natural Science Foundation Outstanding Youth Foundation in 2015.